A comprehensive methodology for computational fluid dynamics combustion modeling of industrial diesel engines

Tommaso Lucchini[1], Augusto Della Torre[1], Gianluca D'Errico[1], Angelo Onorati[1], Noud Maes[2], Lambertus MT Somers[2] and Gilles Hardy[3]

Abstract
Combustion control and optimization is of great importance to meet future emission standards in diesel engines: increase in break mean effective pressure at high loads and extension of the operating range of advanced combustion modes seem to be the most promising solutions to reduce fuel consumption and pollutant emissions at the same time. Within this context, detailed computational fluid dynamics tools are required to predict the different involved phenomena such as fuel–air mixing, unsteady diffusion combustion and formation of noxious species. Detailed kinetics, consistent spray models and high quality grids are necessary to perform predictive simulations which can be used either for design or diagnostic purposes. In this work, the authors present a comprehensive approach which was developed using an open-source computational fluid dynamics code. To minimize the pre-processing time and preserve results' accuracy, algorithms for automatic mesh generation of spray-oriented grids were developed and successfully applied to different combustion chamber geometries. The Lagrangian approach was used to describe the spray evolution while the combustion process is modeled employing detailed chemistry and, eventually, considering turbulence–chemistry interaction. The proposed computational fluid dynamics methodology was first assessed considering inert and reacting experiments in a constant-volume vessel, where operating conditions typical of heavy-duty diesel engines were reproduced. Afterward, engine simulations were performed considering two different load points and two piston bowl geometries, respectively. Experimental validation was carried out by comparing computed and experimental data of in-cylinder pressure, heat release rate and pollutant emissions (NO_x, CO and soot).

Introduction

High efficiency and reliability make diesel engines the favorite choice of heavy-duty applications for road transportation, agriculture and many industrial applications. Fulfillment of emission standards and, at the same time, fuel consumption reduction currently drive the design and development of new compression-ignition (CI) engines. Possible improving areas are represented by turbocharging, air management, combustion and after-treatment systems.[1,2] When focusing on combustion, currently efforts are focused on the increase in the compression ratio and injection pressure.[3] To exploit all the advantages of such solutions, combustion chamber geometry optimization is also necessary and this requires a deep understanding of the complex interplay of the complex physical processes governing fuel–air mixing, flame propagation and formation of pollutants.[4]

To this end, computational fluid dynamics (CFD) is applied for combustion system design. However, to be predictive and massively usable for engine design, a CFD code must fulfill different pre-requisites with the

[1]Department of Energy, Politecnico di Milano, Milano, Italy
[2]Technische Universiteit Eindhoven, Eindhoven, The Netherlands
[3]FPT Motorenforschung AG, Arbon, Switzerland

Corresponding author:
Tommaso Lucchini, Department of Energy, Politecnico di Milano, Via Lambruschini, 4, 20156 Milano, Italy.
Email: tommaso.lucchini@polimi.it

most important ones being the capability to automatically generate the computational mesh and the availability of accurate and robust numerical methods. Furthermore, extensively validated physical models are necessary to describe spray evolution, combustion with turbulence–chemistry interaction and pollutant formation.[5,6]

This work is focused on the development of a comprehensive methodology for CFD simulation of heavy-duty diesel engines using the Lib-ICE code, which is based on the OpenFOAM technology. Suitable algorithms were developed to automatically generate spray-oriented grids on the basis of engine geometry data. The proposed mesh structure minimizes numerical diffusivity where fuel–air mixing process takes place, creating the possibility to perform simulations with an acceptable grid size.[7] The spray is modeled with the Lagrangian approach, including suitable sub-models for turbulent jet atomization and secondary breakup.[8] Diesel combustion is assumed to be represented by a multiple number of diffusion flames evolving in the mixture fraction space with turbulence–chemistry interaction governed by the scalar dissipation rate. Suitable sub-models for prediction of pollutant emissions were also introduced and their coupling with the combustion was extensively discussed.

A comprehensive validation of the proposed approach was carried out considering two separate steps. The main objective of the first one was to verify the capability of the employed set of models to reproduce spray evolution and flame structure. To this end, the experiments were carried out at the Eindhoven Technical University using a combustion vessel in which it is possible to reach ambient conditions typical of heavy-duty engines at full load. The fuel is delivered by a single-hole, large nozzle, and a set of different operating conditions were used for a full characterization of the fuel–air mixing and combustion processes. Afterward, engine simulations were carried out considering two different engine geometries, producing the same amount of power and NO_x for the two selected operating points. Validation is carried out by a comparison between computed and experimental data of in-cylinder pressure, heat release rate (HRR) and pollutant emissions (NO_x, CO, soot).

Computational models

Fuel–air mixing simulations were carried out using the Lib-ICE code, which is a set of libraries and solvers for IC engine modeling based on the OpenFOAM technology. Over the years, it was successfully applied to simulation of spray and combustion in direct-injection engines.[7,9,10]

Spray model

Due to the relatively large nozzle sizes employed in heavy-duty engines, higher spray penetrations are expected, and to achieve realistic results the CFD setup is crucial in terms spray sub-models, mesh size and turbulence. In particular, atomization and breakup spray sub-models regulate the droplet size evolution once they have left the nozzle with a consequent effect on mass and momentum transfer to the gas phase. Due to longer spray penetrations, Lagrangian and Eulerian phases are expected to interact over a larger portion of the computational domain. Hence, mesh size and structure must be carefully chosen due to the well-known grid dependency problem. Following previous works,[10,11] separate models were applied to predict atomization and secondary breakup processes. This is expected to better reproduce the morphology and the evolution of sprays emerging from large nozzles. The Huh–Gosman model was used[8] for spray atomization: primary parcels (blobs) are injected into the computational mesh with the same nozzle diameter and their velocity is function of the injected mass flow rate profile. Both Kelvin–Helmholtz and turbulence-induced breakup on the jet surface are taken into account by the model, describing the diameter reduction in the injected parcels as function of the characteristic atomization length and time-scales L_a and τ_a whose values are computed at nozzle exit and then change according to the jet turbulence decay. As a consequence of the parent droplet diameter reduction, new droplets are created whose size is computed from a probability density function (PDF) distribution, whose properties follow the one of the expected turbulence length-scale spectrum. The atomization process is supposed to cease as soon as one of the following conditions is satisfied: parent droplet diameter lower than the atomization length scale, Weber number (*We*) lower than 40 or Ohnesorge number (*Oh*) greater than 2. Parent droplets are not subject to drag, evaporation and heat transfer. To better reproduce the atomization process, primary parcels' velocity has the same direction of the nozzle axis. At the time the stripping process takes place, secondary droplets are deflected with a radial velocity $v_r = L_a \tau_a$, which takes into account both turbulence at the nozzle exit and its progressive decay when traveling downstream. This is expected to better predict the spray morphology resulting from atomization.

The model originally proposed by Pilch and Erdman[12] was applied in this work to predict the secondary breakup process. According to their approach, there is a maximum stable diameter D_s below which breakup does not take place. The value of D_s is affected in two ways: (1) the decrease in droplet Weber number because of the new smaller droplet diameter and (2) the decrease in relative velocity between the droplets and the flow field, due to the changes in droplet acceleration (as a result of the decreased droplet diameter). The droplet breakup occurs if the decrease in Weber number is greater than a critical value We_c, accounting for the viscous effects parameterized by the Ohnesorge number.

Representative interactive flamelet combustion model

This model is based on the laminar flamelet concept, assuming that the smallest turbulent time and length scales are much larger than the chemical ones and there exists a locally undisturbed sheet where reactions occur.[13] This sheet can be treated as an ensemble of stretched counter-flow diffusion flames, called *flamelets*. The advantage of such treatment is that all reacting scalars only depend on the mixture fraction variable, Z, which is related to the local fuel-to-air ratio for non-premixed combustion. Hence, local chemical composition can be estimated from the Z field in the CFD domain, assuming that its sub-grid distribution can be represented by a β-PDF. To this end, transport equations for both Z and its variance $\widetilde{Z''^2}$ need to be solved. The Z transport equation includes a source term related to spray evaporation, while such effects are neglected in the mixture fraction variance equation since they do not significantly affect the computed results.

The local flame structure is defined by the flamelet equations for chemical species and enthalpy which are solved assuming unity Lewis number in the mixture fraction space[5] where the effects of turbulence and flow field are grouped into the scalar dissipation rate term

$$\chi_z = \widehat{\chi_{st,j}} \frac{f(Z)}{f(Z_{st})} \tag{1}$$

$f(Z)$ has an ln-profile,[14] while scalar dissipation rate at stoichiometric mixture fraction conditions $\widehat{\chi_{st,j}}$ for each flamelet is computed as an average of the local values in each computational cell and accounting for flamelet marker distribution M_j

$$\widehat{\chi_{st,j}} = \frac{\int\limits_V M_j \chi_{st,l}^{3/2} \rho P(Z_{st}) dV'}{\int\limits_V M_j \chi_{st,l}^{1/2} \rho P(Z_{st}) dV'} \tag{2}$$

where P is the β-PDF of the mixture fraction, whose parameters depend on mixture fraction and its variance.[15] In each cell, $\chi_{st,l}$ is computed following the Hellstrom formulation[16]

$$\chi_{st,l} = \frac{\chi}{\int\limits_0^1 \frac{f(Z)}{f(Z_{st})} \tilde{P}(Z) dZ} \tag{3}$$

The chemical composition in each cell of the CFD domain is thus computed from mixture fraction and its variance distribution as follows

$$Y_i(\vec{x}) = \sum_{j=1}^{N_f} M_j \int_0^1 Y_{j,i}(Z) P(Z, \widetilde{Z''^2}) dZ \tag{4}$$

In case a multiple number of flamelets is employed, M_j in equation (4) represents the so-called *flamelet marker* field in the CFD domain.[5,17]

One of the advantages of the representative interactive flamelet (RIF) model compared to other ones based on detailed chemistry is represented by the fact that the reaction–diffusion problem is solved in the mixture fraction space, which is approximated as a one-dimensional grid with a limited number of points (100–200). This drastically reduces the CPU time required for chemistry integration and makes possible to use large mechanisms (more than 100 species) with a better prediction of both combustion and pollutant emissions. A single flamelet was used to represent diesel combustion and this choice was motivated by the very short ignition delays which are typical of the chosen operating conditions. The use of a single flamelet was also supported by a preliminary sensitivity analysis carried out by the authors: no relevant changes in computed cylinder pressure and NO_x results were found when using up to 20 flamelets. At the beginning of the simulation, the temperature profile in the mixture fraction space is initialized from enthalpy balance assuming oxidizer temperature at $Z = 0$ and $380\,K$ temperature at $Z = 1$

$$h(Z) = (1 - Z) \cdot h(Z = 0) + Z \cdot h(Z = 1) \tag{5}$$

It is also possible to take the fuel evaporation into account during initialization, but for the tested conditions in this work no significant changes were found and for this reason this effect was not considered.

Prediction of pollutant emissions

Suitable sub-models to estimate the main pollutant emissions formed during the combustion process were also implemented in the proposed framework. In particular, the possibility to predict CO, NO_x and soot was included. Carbon monoxide concentration is directly estimated from the flamelet domain. This choice is justified by the fact that in the diffusive combustion process, CO is formed where the mixture is rich and then convected by flow and turbulence in lean regions where it is oxidized. Hence, CO mass fraction is evaluated consistently with Eq. (4) as follows

$$Y_{CO}(\vec{x}) = \sum_{j=1}^{N_f} M_j \int_0^1 Y_{j,CO}(Z) P(Z, \widetilde{Z''^2}) dZ \tag{6}$$

NO_x emissions are considered to be only NO and such species is assumed to be formed with the extended Zeldovich mechanism as follows

$$N + NO \leftrightarrow N_2 + O \tag{7}$$
$$N + O_2 \leftrightarrow NO + O \tag{8}$$
$$N + OH \leftrightarrow NO + H \tag{9}$$

Reaction rate constants are taken from Heywood[18] after verifying that suggested values from newer works produce very similar results. Incorporation of NO formation mechanism inside the RIF combustion model is still an open-issue since the time-scales for NO

formation are much longer than the ones of the other species involved in the diffusive combustion process. Evolution of NO inside the cylinder is related to fuel and temperature distributions with the maximum concentrations expected in the high-temperature regions and where the mixture fraction is close to the stoichiometric value. To take such aspects into account, different approaches were proposed in the past[19] and three different methods were implemented in Lib-ICE and compared in this work.

- Model 1: a transport equation for *NO* mass fraction Y_{NO} is solved in the CFD domain and its reaction rate is directly taken from the flamelet domain presuming a β-PDF. Advantage of such approach is represented by its consistency with the RIF combustion model and the possibility to take in-cylinder mixture fraction distribution effects into account. Temperature stratification is not considered, since *NO* reaction rate depends only on the flamelet temperature profile. As a consequence, NO formation rate depends mainly on in-cylinder pressure: as soon as it starts to decrease, NO formation is reduced as well irrespectively of its local concentration and the in-cylinder temperature distribution.
- Model 2: a transport equation for *NO* mass fraction Y_{NO} is solved in the CFD domain with a source term computed in any cell accounting for the average temperature and species concentrations estimated from equation (4) except *NO* for which the local concentration is used. This model can take in-cylinder temperature distribution into account but, on the other hand, it does not consider turbulence–chemistry interaction. For this reason, it is expected that NO will form only in cells where the mixture fraction is stoichiometric and cell temperature is high enough.
- Model 3: the concentration of NO is directly estimated from equation (4). In such case, evolution of NO depends on flamelet temperature history and mixture fraction distribution. This model neglects the time-scales which are typical of NO formation: as a consequence of this, predicted NO concentrations are higher than the ones of the other tested approaches and also of experimental data as reported in Felsch et al.[19]

Soot emissions. The semi-empirical model proposed by Lindstedt and colleagues[20] is used to estimate soot emissions: two transport equations for soot particle number density N_p and volume fraction f_v are solved, with source terms related to nucleation, coagulation, surface growth and oxidation processes as follows

$$\dot{\omega}_{N_p} = \dot{\omega}_{inc} - \dot{\omega}_{coag} \tag{10}$$

$$\dot{\omega}_{f_v} = \dot{\omega}_{inc} + \dot{\omega}_{grow} - \dot{\omega}_{oxi, O_2} - \dot{\omega}_{oxi, OH} \tag{11}$$

Inception and surface growth source terms ($\dot{\omega}_{inc}$ and $\dot{\omega}_{grow}$, respectively) depend linearly on the soot precursor concentration which is considered to be acetylene, consistently with other articles in which the same model was successfully applied to diesel combustion.[21] As it has been experimentally observed, the reactivity of the soot particles decreases in time; in this work, in a consistent way with the original work from Lindstedt and colleagues,[20] this aspect was accounted for by assuming the soot surface growth rate proportional to the square root of the specific surface area, S_{soot}. Coagulation of soot particles $\dot{\omega}_{coag}$ is modeled using the normal square dependence.[20] Soot oxidation depends on O_2 and OH concentrations, following.[20] It is well known that the formation of soot is rather a slow process compared to the other species involved in the combustion chemistry, thus the fast chemistry assumption, solving f_v and N_p equations in the mixture fraction space, might be questionable when it is necessary to predict the effects of mixture distribution, injection pressure and combustion chamber geometry.[22] For this reason, transport equations for the soot model are solved in the CFD domain, and source terms are computed on the basis of the local species concentrations and thermodynamic conditions.

Experimental validation

Two different operating points, named *A75* and *Cruise*, were chosen as representative of the conditions of interest for the design of a heavy-duty truck engine. Minimum fuel consumption is reached in the A75 point, while the Cruise load is typical of constant speed operation in highways. Details related to injection pressure, conditions at start of injection (SOI), engine speed and break mean effective pressure (BMEP) are illustrated in Table 1.

Preliminary assessment and validation of the proposed methodology is necessary with well-documented experiments to successfully apply it also to engine simulations. For this reason, constant-volume conditions were first considered and, in particular, data sets from two different laboratories were used. Fuel–air mixing and combustion experiments carried out in the TU-Eindhoven (TU/e) vessel allowed to assess the proposed set of spray and combustion models at ambient conditions and with nozzle sizes which are typical of heavy-duty diesel engines at SOI time. Measurements recently

Table 1. Details about A75 and Cruise operating points.

	Cruise	A75
Engine speed (r/min)	1200	1200
BMEP (bar)	9.5	19
EGR rate (%)	8	3–6
Injection pressure (bar)	900–1000	1100–1200
Density at SOI (kg/m³)	30	45
Estimated T at SOI (K)	950	1000
Nozzle diameter (μm)	~200	

BMEP: break mean effective pressure; EGR: exhaust gas recirculation; SOI: start of injection.

Table 2. Details of the operating conditions tested in the TU/e high-pressure vessel.

	C1	C2	C3	C4
Ambient density (kg/m^3)	40	40	40	40
Ambient temperature (K)	900	900	900	900
Ambient pressure (bar)	105	105	105	105
Ambient oxygen concentration (% by vol.)	0	0	21	21
Fuel injection pressure (bar)	800	1600	800	1600
Estimated injection duration (ms)	5.2	4.9	5.2	4.9
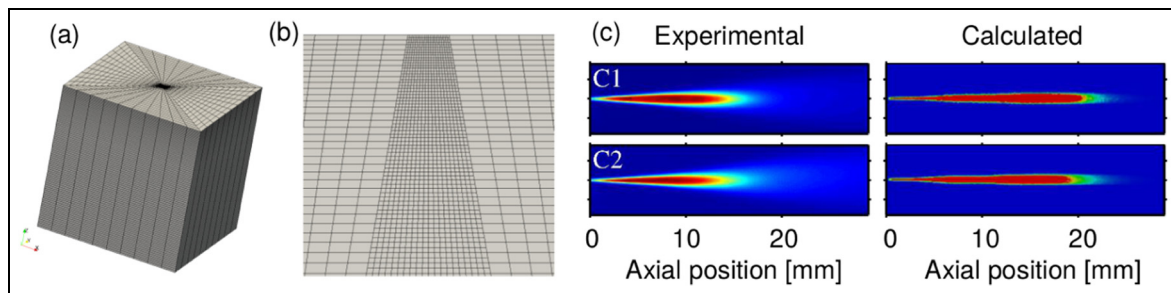
Figure 1. (a) Computational mesh used for fuel–air mixing and combustion simulations in the TU/e vessel. (b) Computational mesh structure in the spray region. (c) Left panel: 2D optical thickness maps obtained with DBI experiments; right panel: numerical reproduction of the optical thickness maps using simulated liquid spray data.

performed in the SANDIA combustion vessel and available in the context of the Engine Combustion Network (ECN)[23] were used to validate the soot model.

All the simulations were run using the standard $k - \varepsilon$ turbulence model whose $C_{\varepsilon 1}$ was slightly increased from 1.44 to 1.5 to better predict the penetration of fuel jets following the practice known as *round jet correction*.[17,24] Diesel fuel in engine simulations was assumed to be n-dodecane, whose oxidation is computed using the mechanism proposed in Chishty et al.[25] which was combined with the Zeldovich mechanism to compute NO. The mechanism has 58 species and 272 reactions. The RIF model equations are solved using the finite volume method in the mixture fraction space which is discretized with 130 grid points, most of them located around the stoichiometric mixture fraction value.

TU/e combustion vessel

Fuel jet experiments were conducted in a constant-volume vessel with optical access where it is possible to reach thermodynamic conditions which are similar to those encountered in heavy-duty diesel engines at full-load conditions.[26] A single-hole common-rail injector is mounted at the center of one of the metal side ports. The injector in this work has an orifice outlet diameter of 205 μm, a converging hole with K-factor 1.5. The high-pressure n-dodecane jets can be visualized through sapphire windows with a diameter of 100 mm from all side ports of the combustion vessel. The vessel is equipped with a pressure transducer, and three different line-of-sight diagnostic techniques were used in this study to obtain ensemble average high-speed

recordings. High-speed liquid- and vapor-phase fuel penetration were measured for non-reacting experiments using diffused, back-illumination (DBI) and Schlieren, respectively. Further details about the employed optical techniques can be found here.[27,28] The experimental results reported in this work were constructed using ensemble averages of at least 10 individual recordings. To determine the HRR, gas pressure measurements were conducted at 50 kHz using a Kistler model 6045A pressure transducer, placed in one of the upper corners opposite to the injector. Four different operating conditions were considered, displayed in Table 2. All of them are well representative of the engine operating points displayed in Table 1 and they differ in terms of injection pressure. C1 and C2 are non-reacting, while for C3 and C4 the ambient oxygen concentration is 21%.

The simulations were carried out using a three-dimensional cubical computational mesh whose volume is very close to the one of the TU/e vessel. Figure 1(a) and (b) illustrates the structure of the computational mesh used in the simulations which intends to reproduce the topology that is commonly adopted to model diesel engine combustion chambers. To better predict the fuel–air mixing process, local refinement was used in the region where the spray evolves, where mesh size ranges from 0.3 to 1 mm. The spray model presented in this work was extensively validated in Maes et al.,[27] where a suitable methodology for a consistent comparison between computed and DBI experimental data of liquid penetration was also developed. In particular, a light scattering model was implemented by the authors following the recent methods suggested by Magnotti
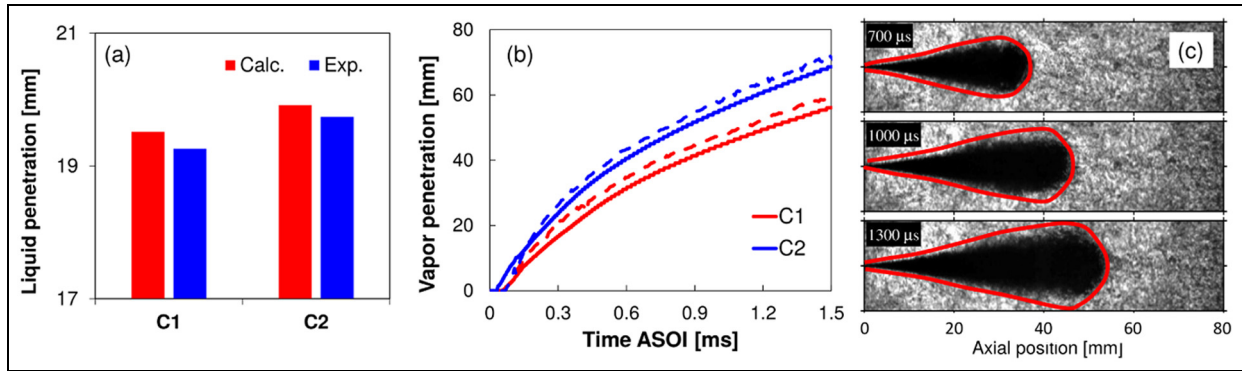
Figure 2. Spray model validation for the C1 and C2 conditions: (a) comparison between experimental and calculated liquid penetration values, (b) comparison between computed (dashed lines) and experimental (solid lines) data of vapor penetration and (c) time sequence of ensemble averaged Schlieren experiments at C1 conditions. The contours represent a numerical mixture fraction threshold of 10^{-3}.

and Genzale.[29] The axial profiles of non-dimensional optical thickness τ^* were computed assuming the spray to be composed only of spherical liquid droplets. For the computation of the steady-state liquid length, the experimental and computed optical thickness profiles were processed in the same way: a line is fitted through the decreasing computed τ^* profile along the injector axis, and the intersection of that line with the abscissa represents the steady-state liquid length. Figure 1(c) compares the computed and experimental optical thickness maps for the C1 and C2 conditions. Steady-state spray penetration is correctly estimated by the simulations, despite its angle looking smaller compared to the experiments.

For further details related to the computation of the liquid penetration value and its comparison with the experimental data, the reader is referred to Maes et al.,[27] where the effects of spray model constants on the computed extinction profiles are presented in detail.

Consistent with Figure 1(b), the computed and experimental data of steady-state liquid penetration agree well as it is illustrated in Figure 2(a) where it is possible to see that the variation in injection pressure from 800 to 1600 bar produces a slight increase in the liquid length for the C2 condition. However, due to the much higher momentum transferred to the gas phase, C2 has a higher vapor penetration compared to C1, and this aspect is correctly predicted by the proposed CFD setup as can be seen in Figure 2(b). The capability to reproduce the vapor distribution was also verified in Figure 2(c) for the C1 condition where computed contours of mixture fraction equal to 10^3 were superimposed to ensemble averaged Schlieren images of fuel vapor at different instants after the SOI. Computations seem to overestimate the radial vapor diffusion and this aspect can be related to the employed turbulence model.

After a proper assessment of the spray model, combustion simulations were carried out for the C3 and C4 operating points. When using a single flamelet, combustion model validation can be performed only in terms of vessel pressure evolution and HRR profiles. This is

because, in each computational cell, the chemical composition is only related to mixture fraction value and its variance. Hence, after ignition, a diffusion flame will be established in the whole computational domain and it will be almost stabilized at the nozzle exit. For a proper prediction of the lift-off length, it is necessary to employ a multiple number of flamelets.[17]

To remove the uncertainties related to the material properties, thermal inertia and radiation, it was decided to compare the normalized profiles of experimental apparent heat release rate (AHRR) and computed HRR directly estimated from the chemical species reaction rate. Such comparison was performed after verifying that in the simulations the ratio between the cumulative heat released by combustion and the injected fuel mass corresponded to the n-dodecane lower heating value. Figure 3(a) and (b) illustrates a comparison between normalized HRR for both the C3 and C4 conditions. Ignition delay time is very short and, in agreement with the experimental data, it is longer (0.32 vs 0.24 ms) for the C4 condition due to the higher injection pressure which is probably responsible for producing scalar dissipation rate values greater than the extinction one for a longer time.[5] The experiments carried out with a smaller nozzle (0.9 mm) show the opposite trend in terms of injection pressure effect on ignition delay;[9] to better understand this aspect, further investigations are required concerning fuel–air mixing in the early part of the injection process and they will be matter of investigation in a future work. Despite injected mass flow rate profiles reaching their steady-state value approximately at 0.25 ms, the rate of heat release has a progressive increase up to 3 ms and then it stabilizes for the C3 condition while it starts decreasing for C4. The RIF model correctly captures these features which can be ascribed.

SANDIA combustion vessel

Assessment and validation of the proposed methodology for soot prediction was carried out with the
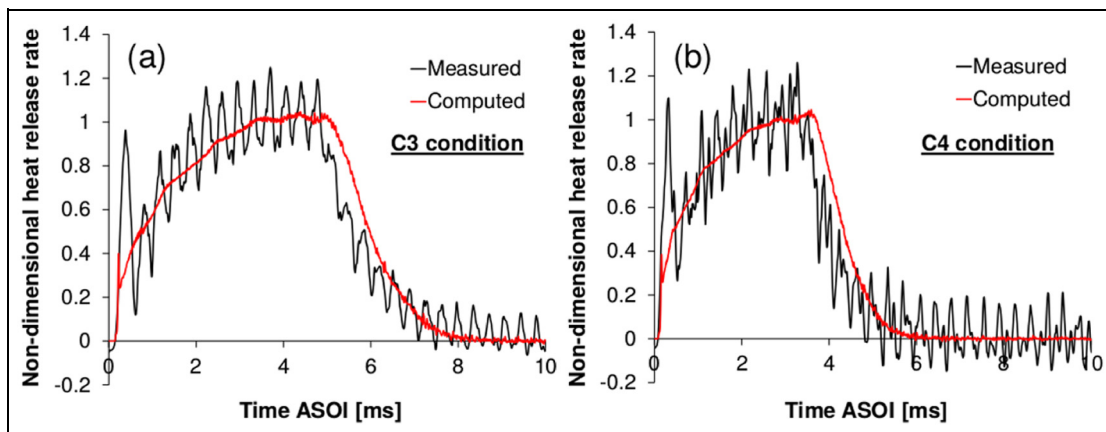
Figure 3. (a) Comparison between computed and experimental values of the normalized heat release rate for the C3 operating condition and (b) comparison between computed and experimental values of the normalized heat release rate for the C4 operating condition.

Table 3. Simulated operating points in the Sandia combustion vessel.

	O3	T3
Oxygen concentration (% by vol.)	21	15
Injection pressure (bar)	1500	1500
Ambient temperature (K)	900	1000
Ambient density (kg/m^3)	22.8	22.8
Injection duration (ms)	5	5

experimental data from the SANDIA combustion vessel which is extensively studied in the context of the ECN.[30] The experimental setup is widely described in Pickett et al.[31] and the so-called *Spray-A* experiment was simulated where n-dodecane is delivered through a single-hole nozzle with a 90-μm diameter and K-factor equal to 1.5. Recently, DBI, extinction imaging (EI) was used to acquire time-resolved images of soot optical thickness (*KL*) in n-heptane spray combustion experiments.[23] DBIEI maps of KL are processed to obtain the dimensional extinction coefficient *K*, which can then be related to the radial distribution of the soot volume fraction f_v.[23] Assuming an axisymmetric jet, the evolution of the total amount of soot can be estimated directly from f_v. Two operating conditions, named *O3* and *T3*, were chosen to test the soot model from Leung, Lindstedt and Jones implemented in Lib-ICE. Details of such conditions are provided in Table 3. They can be considered good candidates for a preliminary validation of the soot model before carrying out engine simulations because they have different ambient temperature and oxygen concentration values.

First, it was verified that combustion simulations reproduce correctly the experimental HRR. In Figure 4(a) and (b), the computed and experimental normalized HRR profiles are compared for the T3 and O3 operating conditions. Highest injection pressure and smaller nozzle size are responsible for a different

development of the combustion process, reaching the steady-state HRR very fast compared to the TU/e vessel. For both the tested conditions, the RIF model correctly reproduce the experimental trend in terms of ignition delay time and transition to steady *injection rate controlled* combustion mode.

The soot model was tuned on the O3 condition by slightly modifying only the pre-exponential factor of the oxidation reactions and using all other constants as originally suggested by Lindstedt and colleagues.[20] Then the model capabilities were verified also for the T3 operating point, having a higher ambient temperature and lower oxygen concentration. The computed and experimental evolutions of soot mass as function of time are reported in Figure 5 for both the considered conditions. Despite only one flamelet being used and, consequently, flame attached to the nozzle, the soot trend is reproduced fairly well for the tested conditions because of the following two separate reasons:

- Acetylene, used as soot precursor species, is formed mainly in the very rich core of the jet which is located far from the nozzle.
- Soot transport equations are solved in the CFD domain and this makes its distribution more consistent with local flow and species concentration.

Despite the authors being aware of the well-known relation between soot distribution and lift-off length and the need to use multiple flamelets for a proper prediction of flame stabilization, they consider this setup suitable for conventional combustion simulations in heavy-duty engines, where very short lift-off lengths are expected due to the high cylinder pressure and temperature values which are generally found.

Finally, Figure 6(a) and (b) displays the computed and experimental distributions of soot volume fraction f_v for the O3 and T3 operating conditions, respectively. Compared to O3, the increase in the ambient
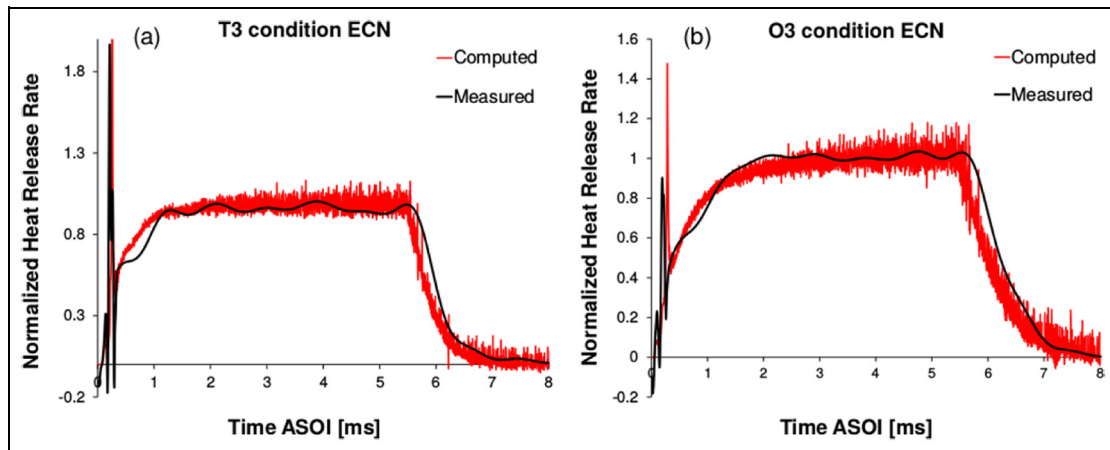
Figure 4. (a) Comparison between computed and experimental values of the normalized heat release rate for the T3 operating condition and (b) comparison between computed and experimental values of the normalized heat release rate for the O3 operating condition.
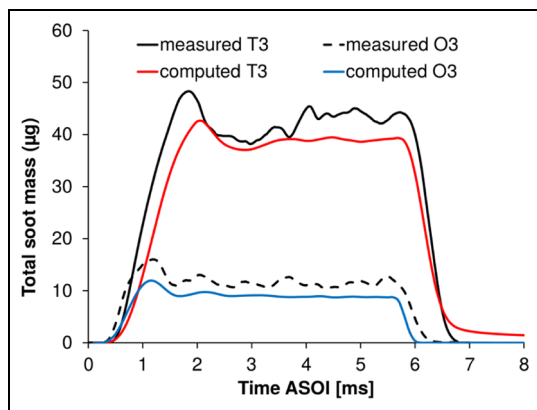

Figure 5. Computed versus experimental evolution of soot mass as function of time for the Spray-A O3 and T3 operating conditions.

there is a larger zone where soot is formed and also that maximum f_v values are higher. These results are very encouraging, since they prove that a combination of the Lindstedt semi-empirical and RIF model allows a rather good description of the soot structure within the flame and of the transient and steady evolution of the soot mass for operating conditions which are typical of conventional diesel combustion, where the reactivity of the fuel is high. Particularly, the latter is considered to be a significant validation, requiring an equilibrium condition among the four sub-mechanisms of soot formation and the occurring mixing and transport phenomena of gaseous species and soot. Further validation is necessary at lower oxidizer temperature and considering higher charge dilution, also to verify whether the proposed setup based on a single flamelet is still valid.

FPT Cursor 11 engine

After the model validation at constant-volume conditions, combustion simulations were carried out for the

temperature and, at the same time, a reduction in the oxygen concentration in T3 are responsible for a higher amount of soot mass. Both the experiments and simulations show in Figure 6(b) that in the T3 condition
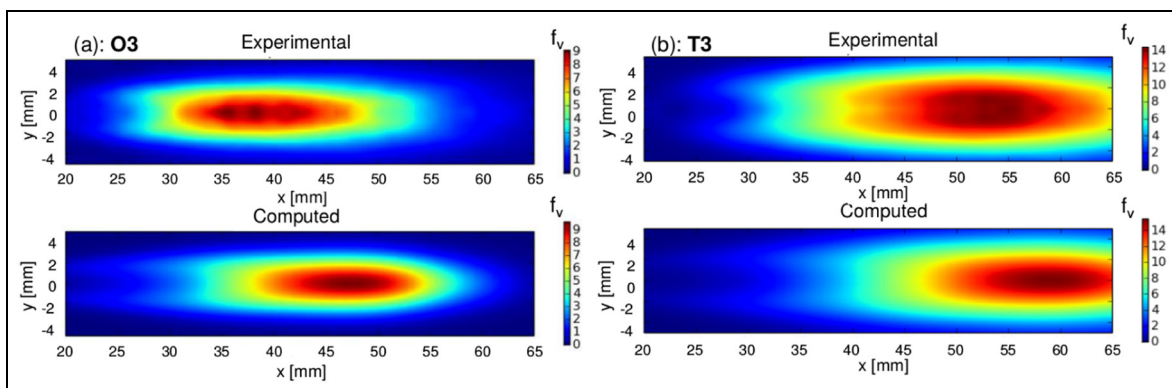

Figure 6. Comparison between experimental (top) and computed (bottom) distributions of soot volume fraction f_v for (a) the O3 operating condition and (b) the T3 operating condition.
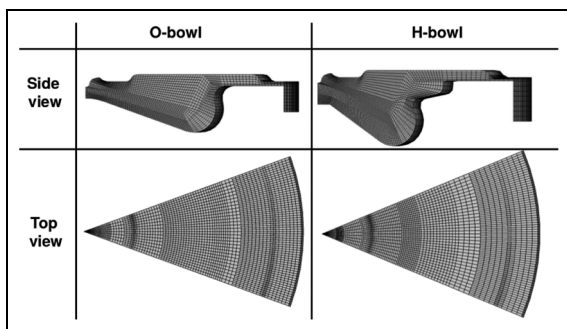
Figure 7. Details of the computational grids used for the combustion simulations in the *O-Bowl* and *H-Bowl* combustion chamber layouts.

Table 4. Tested operating conditions in the FPT C11 engine using the *O-Bowl* and *H-Bowl* configurations.

Bowl type	H-Bowl	O-Bowl	H-Bowl	O-Bowl
Operating condition	A75	A75	Cruise	Cruise
BMEP (bar)	19	19	9.5	9.5
NO/NO_{ref}	1.3	1.3	1	1
Relative air–fuel ratio λ	1.6	1.6	2.0	2.0
SOI (°BTDC)	9.1	6.3	8.0	6.5
Injection pressure (bar)	1100	1200	900	1000
EGR (%)	3.0	6.0	8.0	8.0
Bore (mm)	128			
Stroke (mm)	144			

BMEP: break mean effective pressure; SOI: start of injection; BTDC: before top dead center; EGR: exhaust gas recirculation.

FPT Cursor 11 engine. The effects of combustion chamber geometry were evaluated at different operating conditions. In particular, two different layouts for the piston bowl were tested under the A75 and the Cruise load points. Piston bowl geometry details are provided in Figure 7: the first one is named *O-Bowl* and presents the well-known Mexican Hat layout. The second one has a deeper bowl and it is called *H-Bowl*. It was designed to enhance the air entrainment inside the fuel spray with expected positive effects on combustion efficiency and pollutant emissions. Different cylinder heads and injectors were used: with the O-Bowl, the engine runs with a 0.5 swirl ratio and a nine-hole nozzle while H-Bowl was tested with an eight-hole nozzle and higher swirl (1.3). The compression ratio from the H-Bowl is 20.5 which is slightly higher than the one of the O-Bowl (20); for this reason, SOI time was adjusted to achieve the same BMEP for any load with the two bowl configurations. Same NO_x levels were experimentally achieved from the A75 and Cruise load points, respectively. The details of the operating conditions tested are illustrated in Table 4.

In Figure 7, the computational grids employed for the simulations are reported. They were generated automatically with the algorithm described in Lucchini et al.[7] On the basis of user parameters related to main engine geometry data, combustion chamber layout and spray axis, a spray-oriented mesh is automatically generated. Such grid layout is expected to minimize the numerical diffusivity with positive effects on the prediction of the fuel–air mixing, combustion and pollutant formation processes. The simulations were carried out in a sector of the combustion chamber (1/9 for the O-Bowl and 1/8 for the H-Bowl) and, to keep a fine enough mesh resolution in the whole domain, the grid is progressively refined in the polar direction. At top dead center (TDC), the O-Bowl mesh has approximately 50,000 cells while the 60,000 cells are used for the H-Bowl. Simulation starts from intake valve closing (IVC) where a swirl motion was imposed assuming a wheel-flow velocity profile. Wall-heat transfer is modeled by using the Huh–Chang temperature wall functions.[32] The spray model setup was the same employed for the simulations carried out in the TU/e vessel.

The validity of the combustion model was first verified for the A75 load condition and Figure 8(a)–(d) reports a comparison between the computed and experimental data of in-cylinder pressure and HRR profiles for both the tested piston bowl configurations. Figure 8(a) and (b) shows that the calculated cylinder pressure trace matches well with the experimental one for both the H- and O-Bowl geometries. In the H-Bowl, the fuel is injected later, and to compensate this delay the injection pressure is increased by approximately 100 bar. The result of this is a more rapid growth of the HRR profile after ignition delay, as well as higher values during the part where HRR reaches almost a constant value. Both these features are well reproduced by the RIF model as it can be seen comparing Figure 8(c) and (d).

In the Cruise condition, due to the reduced engine load, injection is shortened and the experimental HRR profile assumes a sort of triangular shape with the maximum value located shortly after the TDC. The results for the H-Bowl, presented in Figure 9(b)–(d), are satisfactory and qualitatively similar to what was achieved for the A75 load point. Computed HRR ramp is steeper than the experimental one, but the location and magnitude of maximum HRR are very well predicted as well as the in-cylinder pressure trace. O-Bowl results in the Cruise load point are not satisfactory and they need to be further analyzed. Figure 9(a) shows that the computed cylinder pressure is underestimated and the peak value is located before where it was found in the experiments. The comparison between the calculated and experimental values of the HRR in Figure 9(b) shows that combustion is very slow after auto-ignition.

To improve O-Bowl results, a deeper analysis will be carried out in the future by analyzing both fuel–air mixing and combustion processes with both the experiments and simulations.

The effect of engine load on CO emissions is reported in Figure 10(a) and (b) for the O-Bowl and H-Bowl configurations. For sake of completeness, the benefits of using the H-Bowl to reduce CO emissions
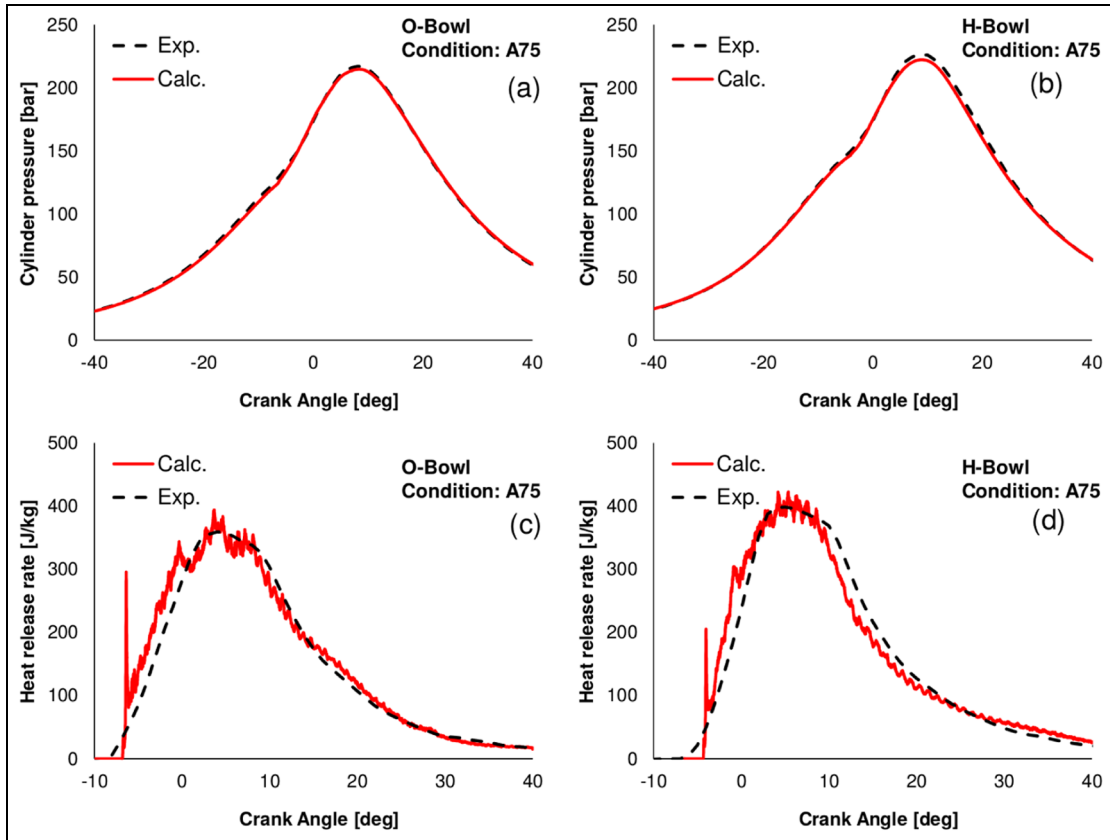
Figure 8. A75 load point. Comparison between computed and experimental in-cylinder pressure profiles for (a) O-Bowl configuration and (b) H-Bowl configuration; comparison between computed and experimental in heat release rate profiles for (c) O-Bowl configuration and (d) H-Bowl configuration.
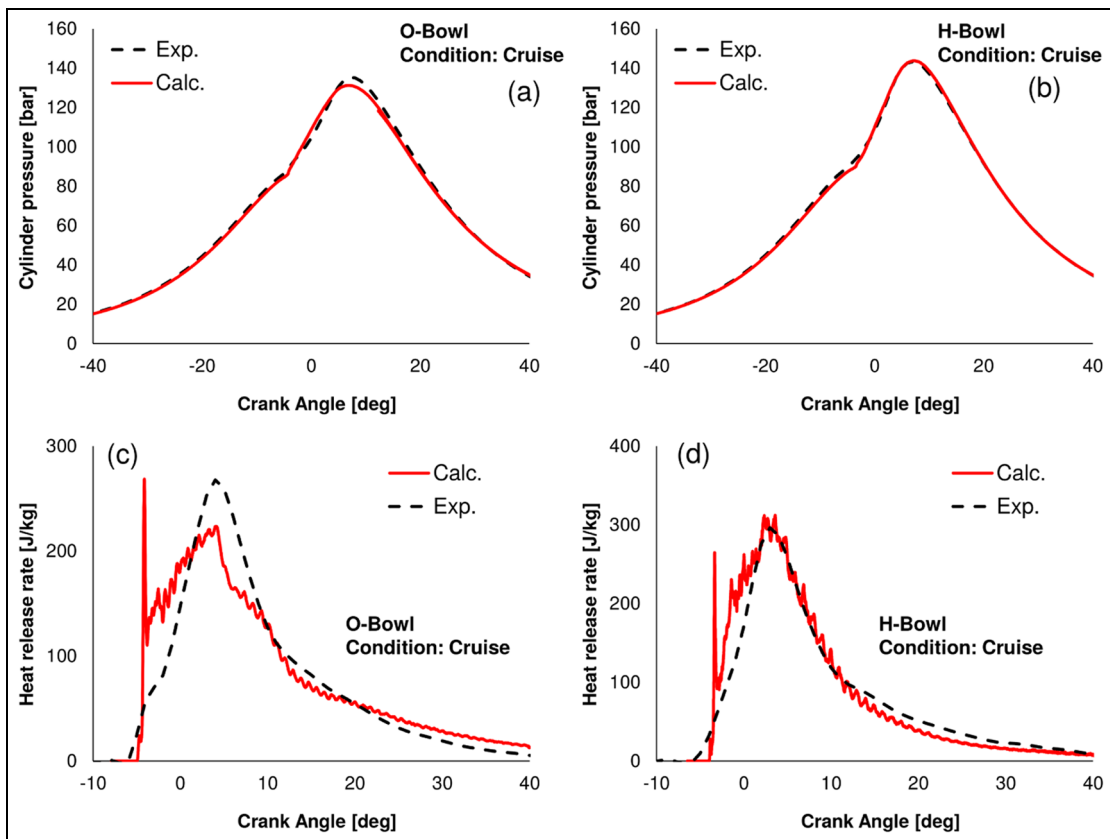

Figure 9. Cruise load point. Comparison between computed and experimental in-cylinder pressure profiles for (a) O-Bowl configuration and (b) H-Bowl configuration; comparison between computed and experimental in heat release rate profiles for (c) O-Bowl configuration and (d) H-Bowl configuration.
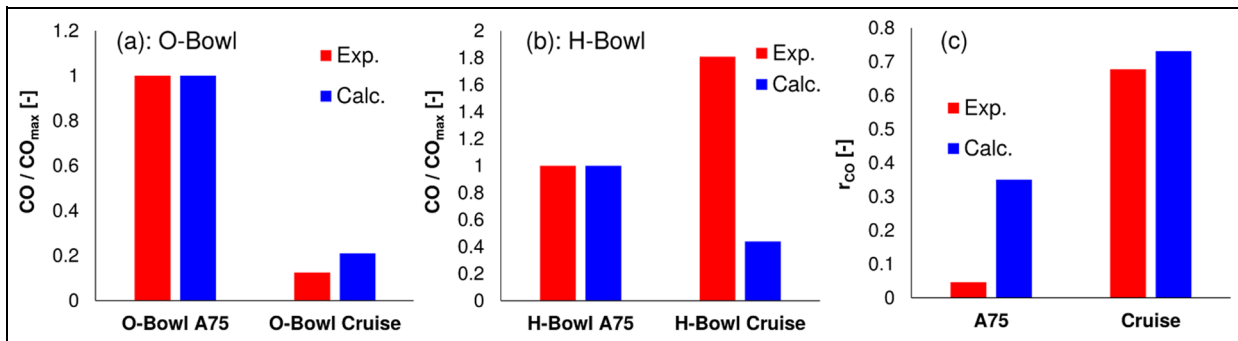
Figure 10. (a) Comparison between normalized computed and experimental CO emissions for the O-Bowl condition, (b) comparison between normalized computed and experimental CO emissions for the H-Bowl condition and (c) comparison between computed and experimental r_{CO} values for the A75 and Cruise load points.
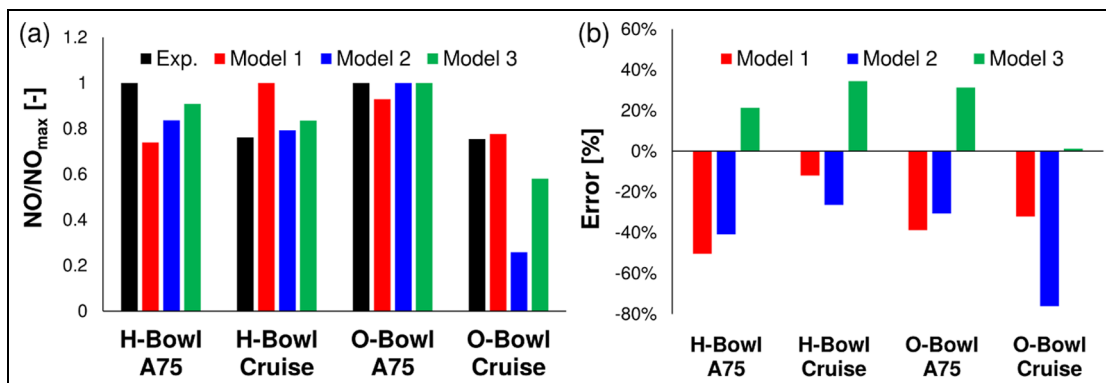

Figure 11. (a) Comparison between experimental and computed normalized NO_x emissions from Models 1, 2 and 3 and (b) computed relative error in NO_x estimation from Models 1, 2 and 3.

are also reported for the experiments and simulations in Figure 10(c) where the non-dimensional ratio

$$r_{CO} = \frac{CO_{H-Bowl}}{CO_{O-Bowl}} \tag{12}$$

is shown. It is possible to see that under the A75 operating condition, the H-Bowl is capable of an approximately 90% reduction in CO emissions compared to O-Bowl. The reduction in CO emissions for the O-Bowl from A75 to Cruise load point is correctly estimated by the simulations in Figure 10(a) and the main reason for this trend seems to be the increase in the relative air–fuel ratio λ. Figure 10(b) shows a different behavior for the H-Bowl configuration where levels of CO for the two load points are very similar and much less depending on the relative air–fuel ratio. Even CO emissions for the A75 load point are lower than the ones reported for the Cruise condition. Figure 10(b) shows that the simulations predict the opposite trend. However, analyzing only Figure 10(a) and (b) would lead to wrong conclusions in terms of the model capabilities to predict CO. Looking again at Figure 10(c), it is possible to see the r_{CO} parameter for the Cruise load point is correctly predicted and also for the A75 condition simulations predict a reduction in CO emissions by approximately 65% instead of 90% reported in the experiments. From

this investigation, it is possible to conclude that the proposed approach is able to predict the effects of piston bowl geometry on CO emissions. To further improve the computed results, probably a more detailed study of flow at IVC is necessary for the H-Bowl configuration since combustion simulations reveal that probably the estimated in-cylinder turbulence is higher than the expected one.

The influence of the approach chosen to predict NO_x is reported in Figure 11. In particular, Figure 11(a) reports the normalized NO values with respect to the maximum one, and in Figure 11(b) the relative error with respect to the experimental data is shown. The results provided by Model 1 are not satisfactory: the reduction in load for the H-Bowl corresponds to an increase in NO_x. The trend is instead captured for the O-Bowl conditions. Model 1 always underestimates the experimental NO_x values consistently with what was discussed when it was presented: it can take into account turbulence–chemistry interaction but, on the other hand, it neglects in-cylinder temperature distribution. This seems to be an important drawback mainly for the H-Bowl configuration. The trend of NO_x from Model 2 is in better agreement with the experimental data since the reduction in NO_x from A75 to Cruise load is correctly predicted. The computed data are

underestimated also for this model, and the reason for this seems to be related to the fact that NO reaction rate depends on the average cell temperature and composition. Except for the O-Bowl case under the cruise load, where cylinder pressure is underestimated, the results from Model 3 overestimate the experimental data by a 20% factor, but they are the ones which better reproduce the experimental trend either in terms of NO variation as function of load and the piston bowl design. For this reason, Model 3 is probably the best for engine design purposes. Unfortunately, because of an unexpected lack of available measurements, it was not possible to carry on a validation of the proposed soot model in the engine conditions.

Conclusion

This work was focused on the development of a comprehensive methodology for the simulation of heavy-duty diesel engines. To this end, sub-models for spray and combustion and mesh management were implemented in the Lib-ICE code and assessed, aiming at the definition of the best numerical approach to estimate soot, NO_x and CO emissions. Dedicated constant-volume experiments were carried out at conditions similar to those encountered in heavy-duty engines using an equivalent single-hole injector, to verify the capability of spray and combustion models to correctly reproduce both air–fuel mixing and HRR. The soot model instead was validated on the basis of the measurements of soot distribution taken in the ECN Spray-A experiments. Afterward, engine simulations were carried out.

The achieved results illustrate that the proposed methodology can be successfully applied for design of heavy-duty diesel engines, since it is capable to reproduce the effects of piston bowl geometry and operating conditions on both combustion and pollutant emissions. However, there are some open issues which require further investigation and will be the matter of study in future works, namely

- Mesh structure and resolution: the proposed algorithm for automatic mesh generation produces grids of acceptable size and quality, ensuring accurate results. Possible further improvements could be focused on a better control of the mesh resolution where spray evolves and ignition takes place.
- NO_x model: the main implications due the way the NO_x chemistry is solved were extensively discussed. However, among the tested alternative approaches, none of them seems to be capable to reproduce the exact NO_x levels, while the correct qualitative trend was observed only assuming fast chemistry.

Declaration of conflicting interests

The author(s) declared no potential conflicts of interest with respect to the research, authorship and/or publication of this article.

References

1. Hashimoto M, Aoyagi Y, Kobayashi M, Murayama T, Goto Y and Suzuki H. BSFC improvement and NOx reduction by sequential turbo system in a heavy duty diesel engine. SAE paper 2012-01-0712, 2012.
2. Yu W, Liu B, Li Y, Su Q, Pei Y and Su W. A hybrid combustion control strategy for heavy duty diesel engines based on the technologies of multi-pulse injections, variable boost pressure and retarded intake valve closing timing. SAE paper 2011-01-1382, 2011.
3. Funayama Y, Nakajima H and Shimokawa K. A study on the effects of a higher compression ratio in the combustion chamber on the diesel engine performance. SAE paper 2016-01-0722, 2016.
4. Singh S, Reitz RD and Musculus MPB. Comparison of the characteristic time (CTC), representative interactive flamelet (RIF), and direct integration with detailed chemistry combustion models against optical diagnostic data for multi-mode combustion in a heavy-duty DI diesel engine. SAE paper 2006-01-0055, 2006.
5. Barths H, Hasse C and Peters N. Computational fluid dynamics modelling of non-premixed combustion in direct injection diesel engines. *Int J Engine Res* 2000; 1(3): 249–267.
6. Bode M, Falkenstein T, Chenadec VL, Kang S, Pitsch H, Arima T and Taniguchi H. A new Euler/Lagrange approach for multiphase simulations of a multi-hole GDI injector. SAE paper 2015-01-0949, 2015.
7. Lucchini T, Torre AD, D'Errico G, Montenegro G, Fiocco M and Maghbouli A. Automatic mesh generation for CFD simulations of direct-injection engines. SAE paper 2015-01-0376, 2015.
8. Huh KY and Gosman AD. A phenomenological model of diesel spray atomization. In: *Proceedings of the international conference on multiphase flows*, Tsukuba, Japan, 24–27 September 1991.
9. D'Errico G, Lucchini T, Onorati A and Hardy G. Computational fluid dynamics modeling of combustion in heavy-duty diesel engines. *Int J Engine Res* 2015; 16(1): 112–124.
10. Lucchini T, D'Errico G, Onorati A, Bonandrini G, Venturoli L and Gioia RD. Development and application of a computational fluid dynamics methodology to predict fuel-air mixing and sources of soot formation in gasoline direct injection engines. *Int J Engine Res* 2014; 15(5): 581–596.
11. Lucchini T, Ettorre D, D'Errico G, Brusiani F, Bianchi G, Montanaro A and Allocca L. Experimental and numerical investigation of high-pressure diesel sprays with multiple injections at engine conditions. SAE paper 2010-01-0179, 2010.
12. Pilch M and Erdman CA. Use of breakup time data and velocity history data to predict the maximum size of stable fragments for acceleration-induced breakup of a liquid drop. *Int J Multiphas Flow* 1987; 13(6): 741–757.

13. Peters N. Laminar flamelet concepts in turbulent combustion. In: *Symposium (International) on combustion*, vol. 21, pp. 1231–1250, 1988.

14. Hasse C. *Modellierung der Zundung und Schadstoffbildung bei der dieselmotorischen Verbrennung mit Hilfe eines interaktiven Flamelet-Modells*. PhD Thesis, RWTH Aachen University, Aachen, 1997.

15. Hasse C. *A two-dimensional flamelet model for multiple injections in diesel engines*. PhD Thesis, Technische Hochschule Aachen, Aachen, 2004.

16. Hellstrom T. *RIF implementation and testing*. Technical report 01.07.1996–31.12.1996, 1997.

17. D'Errico G, Lucchini T, Contino F, Jangi M and Bai X-S. Comparison of well-mixed and multiple representative interactive flamelet approaches for diesel spray combustion modelling. *Combust Theor Model* 2014; 18(1): 65–88.

18. Heywood JB. *Internal combustion engine fundamentals*. McGraw-Hill, New York, 1988.

19. Felsch C, Gauding M, Vanegas A, Won H, Luckhchoura V, Peters N, et al. Evaluation of modeling approaches for NOx formation in a common-rail DI diesel engine within the framework of representative interactive flamelets (RIF). SAE paper 2008-01-0971, 2008.

20. Leung K, Lindstedt R and Jones W. A simplified reaction mechanism for soot formation in nonpremixed flames. *Combust Flame* 1991; 87: 289–305.

21. Bolla M, Farrace D, Wright YM, Boulouchos K and Mastorakos E. Influence of turbulence–chemistry interaction for *n*-heptane spray combustion under diesel engine conditions with emphasis on soot formation and oxidation. *Combust Theor Model* 2014; 18(2): 330–360.

22. Kim T and Kim Y. Interactive transient flamelet modeling for soot formation and oxidation processes in laminar non-premixed jet flames. *Combust Flame* 2015; 162: 1660–1678.

23. Manin J, Pickett L and Skeen S. Two-color diffused back-illumination imaging as a diagnostic for time-resolved soot measurements in reacting sprays. *SAE Int J Eng* 2013; 6(1): 1908–1921.

24. Pope SB. An explanation of the turbulent round-jet/plane-jet anomaly. *AIAA J* 1978; 16(3): 279–281.

25. Chishty M, Bolla M, Hawkes E, Pei Y and Hook S. Assessing the importance of radiative heat transfer for ECN spray a using the transported PDF method. *SAE Int J Fuels Lubr* 2016; 9(1): 100–107.

26. Baert R, Frijters P, Somers LMT, Luijten C and de Boer W. Design and operation of a high pressure, high temperature cell for HD diesel spray diagnostics: guidelines and results. SAE paper 2009-01-0649, 2009.

27. Maes N, Dam N, Somers B, Lucchini T, D'Errico G and Hardy G. Experimental and numerical analyses of liquid and spray penetration under heavy-duty diesel engine conditions. *SAE Int J Fuels Lubr* 2016; 9: 108–124.

28. Pickett LM, Kook S and Williams T. Visualization of diesel spray penetration, cool-flame, ignition, high-temperature combustion, and soot formation using high-speed imaging. *SAE Int J Eng* 2009; 2(1): 439–459.

29. Magnotti G and Genzale C. A novel approach to assess diesel spray models using joint visible and X-ray liquid extinction measurements. *SAE Int J Fuels Lubr* 2015; 8(1): 167–178.

30. Meijer M, Somers B, Johnson J, Naber J, Lee S-Y, Malbec LM, et al. Engine Combustion Network (ECN): characterization and comparison of boundary conditions for different combustion vessels. *Atomization Spray* 2012; 22(9): 777–806.

31. Pickett LM, Genzale CL, Bruneaux G, Malbec L-M, et al. Comparison of diesel spray combustion in different high-temperature, high-pressure facilities. *SAE Int J Eng* 2010; 3(2): 156–181.

32. Huh KY, Chang IP and Martin JK. A comparison of boundary layer treatments for heat transfer in IC engines. SAE paper 900252, 1990.